JOINT CENTER FOR SATELLITE DATA ASSIMILATION

NO. 55, SPRING 2017

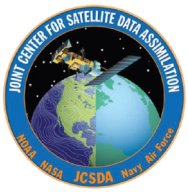

JCSDA Quarterly

NOAA | NASA | US NAVY | US AIR FORCE

doi:10.7289/V5V98648

NEWS IN THIS QUARTER

SCIENCE UPDATE

Global AVHRR Winds Assimilation at Fleet Numerical Meteorology and Oceanography Center/Naval Research Laboratory, Monterey, CA

Atmospheric Motion Vectors (AMVs) from polar-orbiting satellites have been in operational use at Fleet Numerical Meteorology and Oceanography Center (FNMOC) since winds from the Moderate-resolution Imaging Spectro-radiometer (MODIS) produced at the University of Wisconsin were introduced in October 2004. Traditionally, such polar winds are based on imagery from overlapping swaths in successive orbits from a single satellite. Their dependence on overlapping swaths also limits the data to polar regions, typically poleward of 60 degrees. However, the European Organisation for the Exploitation of Meteorological Satellites (EUMETSAT) is taking advantage of having Metop-A and Metop-B in the same orbit (separated by half an orbit) and began operational production of two-satellite AMVs using image pairs in February 2015 (Borde et al. 2016), and using image triplets (A-B-A or B-A-B) in January 2016 (EUMETSAT 2016). The "dual Metop" AMVs are available globally, while the "triplet Metop" join "single Metop" AMVs in polar regions. (Note that at FNMOC, we form superobs for these data without differentiating among single Metop, dual Metop, and triplet Metop wind vectors, instead treating them as a single observation type.) This article describes results from tests of Global AVHRR AMVs in the U.S. Navy's global modeling system, where they have been used operationally since February 2016.

(continued on page 2)

IN THIS ISSUE

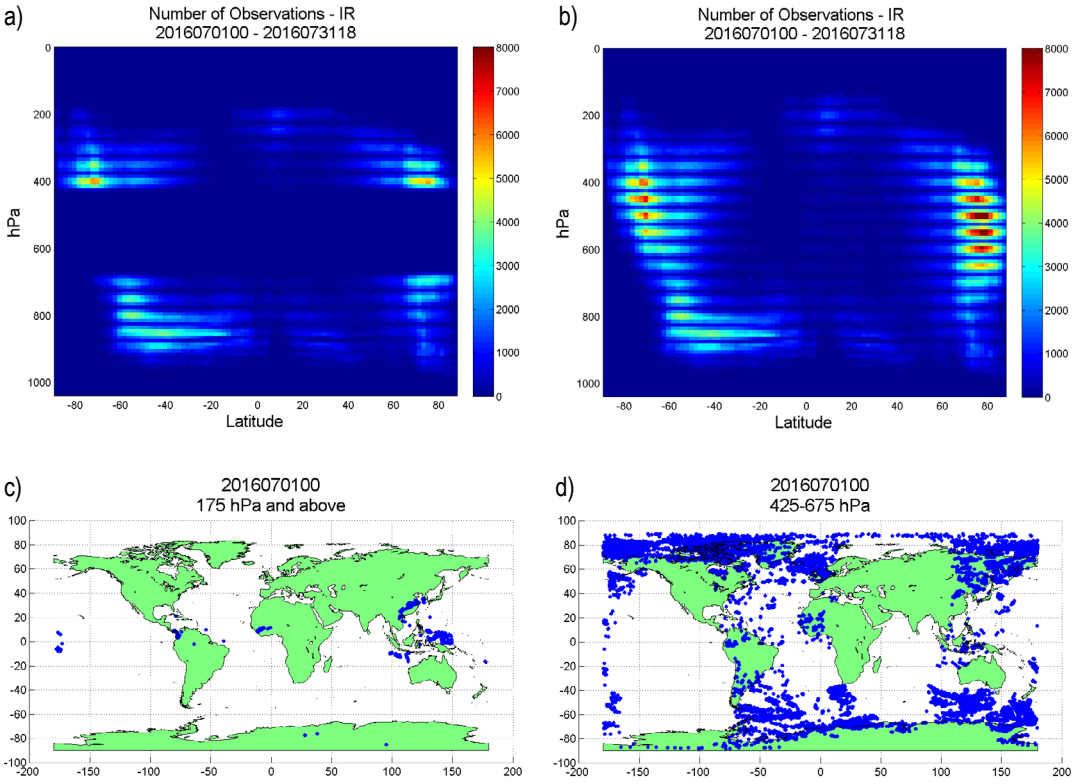

Figure 1. *Meridional slice of zonally averaged data counts of superobbed Global AVHRR winds in the control (a, upper left) and the experiment with relaxed quality control screening (b, upper right). Plotted geographic positions of AMVs assimilated in the experiment but not the control above 175 hPa (c, lower left) and 425-675 hPa (d, lower right) for a single 6-hour data window.*

Atmospheric motion vectors have had large beneficial forecast impact in the U.S. Navy's global operational numerical weather prediction system for many years, so the U. S. Naval Research Laboratory (NRL) and FNMOC continue to aggressively pursue testing and assimilation of new satellite winds datasets. The U.S. Navy's global forecast system is composed of NAVDAS-AR (NRL Atmospheric Variational Data Assimilation System—Accelerated Representer), a hybrid ensemble/4DVAR (four-dimensional variational) global data assimilation system in observation space (Xu et al. 2005; Rosmond and Xu 2006; Chua et al. 2009; Kuhl et al. 2013), and NAVGEM (Navy Global Environmental Model), a global atmospheric model currently run with a resolution of 425 spectral waves with triangular truncation and 60 levels (Hogan et al. 2014). Global AVHRR testing by NRL/FNMOC began in November 2015 and immediately showed beneficial impacts, so these winds were introduced into operations in February 2016. Soon thereafter it was noted (Stone et al. 2016) that some of the data excluded by standard QC procedures looked as if it might also be beneficial, motivating a fresh look at some of the QC measures and a set of test runs which relaxed some of the QC measures.

The control run for our experiment emulated operations as closely as possible. In our tests, we relaxed two routine QC checks that are used in operations. One is a check which screens out incoming AMVs (prior to being superobbed) based on observation-minus-background (OmB) vector differences; the OmB limit ranges from 8–12 m/s, depending on the pressure level of the observation. The other is a check which screens out observations based on their pressure level; all

(continued on page 3)

JOINT CENTER FOR SATELLITE DATA ASSIMILATION

5830 University Research Court
College Park, Maryland 20740

Website: wwws.jcsda.noaa.gov

EDITORIAL BOARD

Editor:
James Yoe

Assistant Editor:
Biljana Orescanin

Director:
Thomas Auligné

Chief Administrative Officer:
James Yoe

AMVs above 175 hPa, below 975 hPa, and almost all AMVs between 425 and 675 hPa are excluded from the assimilation. Our test run *Hnorejvec* bypassed the routine which screens based on OmB vector difference, while the test run *Hnocutout* also bypassed the check against the background, but, in addition, allowed through observations above 175 hPa and between 425 and 675 hPa.

We applied the relaxed QC measures to all sources of AMVs, but Global AVHRR and JMA's Himawari-8 winds were responsible for the great majority of newly admitted data. Most of the mid-level data excluded from the control is in polar and near-polar regions, while most of the upper-level data excluded from the control is in the tropics. Fig. 1 shows data distributions for a typical six-hour data window.

The mean vector difference (MVD) between the observations and the background, one indication of data quality, is plotted in

(continued on page 4)

Figure 2. *Mean Vector Difference (a, upper left) and Forecast Sensitivity Observation Impact (b, upper right) of the control and both experiments, binned by pressure levels. Time series of total FSOI for all vertical levels (c, lower left). Ranking of observation types by total contribution to FSOI during July 2016 (d, lower right).*

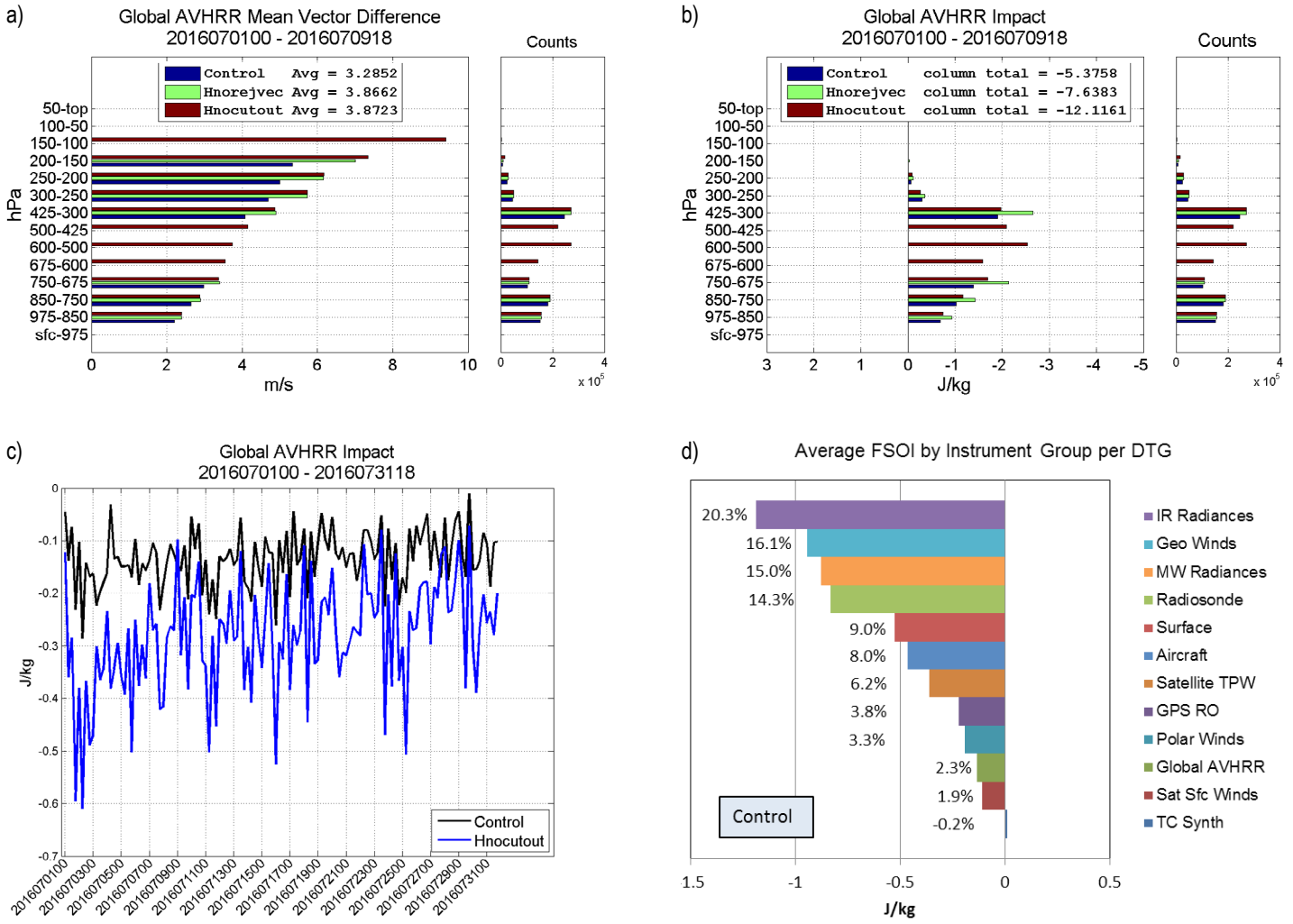

profile in Fig. 2a. The vector differences of AMVs with heights between 425–675 hPa indicate that the data in these mid-levels are comparable in accuracy to the AMVs in the levels above and below. Fig. 2b shows the impact of the data using the Forecast Sensitivity Observation Impact (FSOI) method of Langland and Baker, 2004. Again, the data in mid-levels is comparable in impact, and perhaps even more beneficial than the data above and below because the mid-levels were a relative data void. At upper levels, the newly admitted data has significantly larger MVDs, and while we cannot determine how much of the increase is due to data quality as opposed to background quality, we do see that the counts above 175 hPa are small enough that the beneficial impact at those levels is quite small.

Fig. 2c shows the FSOI due to Global AVHRR AMVs (all levels) for each six-hour analysis data window during the test period July 2016. There were no instances of non-beneficial impacts (as occasionally happens with other instruments, particularly when data counts are low), and the beneficial impact in the *Hnocutout* run was greater than in the control in all but two six-hour windows. In our tests, Global AVHRR's contribution to total FSOI was greater than the contributions from all but one of the geostationary satellite sources. Global AVHRR winds provide approximately 2.3 percent of the total FSOI, which is more than the combined surface satellite-derived winds from ASCAT, SSMIS, and WindSat (Figure 2d).

Because of these positive results, the mid-level cutout for Global AVHRR AMVs was eliminated from the operational suite, allowing these data into the operational analysis, beginning with the update that went in on January 25, 2017. Global AVHRR's upper level cutout and its screening against background values remain in place pending further testing.

Rebecca Stone (SAIC, U.S. Naval Research Laboratory, Monterey, CA), Patricia Pauley (U.S. Naval Research Laboratory, Monterey, CA), Nancy Baker (U.S. Naval Research Laboratory, Monterey, CA), Randal Pauley (Fleet Numerical Meteorology and Oceanography Center, Monterey, CA), Bryan Karpowicz (Devine Consulting, U.S. Naval Research Laboratory, Monterey, CA)

Acknowledgments:
The authors gratefully acknowledge the support from the Office of Naval Research through Program Element PE0603207N. This is NRL contribution NRL/PU/7530-17-074, which is approved for public release and distribution is unlimited.

References

Borde, R., O. Hautecoeur, and M. Carranza, 2016. EUMETSAT Global AVHRR Wind Product. *J. Atmos. Oceanic Technol.*, 33, 429–438, doi: 10.1175/JTECH-D-15-0155.1.

Chua, B., L. Xu, T. Rosmond, and E. Zaron, 2009. Preconditioning representer-based variational data assimilation systems: Application to NAVDAS-AR. *Data Assimilation for Atmospheric, Oceanic and Hydrologic Applications*. Springer-Verlag, pp. 307–320.

EUMETSAT, 2016. The new AVHRR Triplet Mode Polar Winds are available on EUMETCast and the GTS from today (21 January). Accessed February 14, 2017. [Available online at http://www.eumetsat.int/website/home/News/DAT_2903504.html.]

(continued on page 5)

Hogan, T.F., M. Liu, J.A. Ridout, M.S. Peng, T.R. Whitcomb, B.C. Ruston, C.A. Reynolds, S.D. Eckermann, J.R. Moskaitis, N.L. Baker, J.P. McCormack, K.C. Viner, J.G. McLay, M.K. Flatau, L. Xu, C. Chen, and S.W. Chang, 2014. The Navy Global Environmental Model. *Oceanography*, 27(3), 116–125, doi:10.5670/oceanog.2014.73.

Kuhl, D.D, T.E. Rosmond, C.H. Bishop, N.L. Baker, and J. McLay, 2013. Comparison of hybrid ensemble/4D-Var and 4D-Var within the NAVDAS-AR data assimilation framework. *Mon. Wea. Rev.*, 141, 2740-2758.

Langland, R.H., and Baker, N.L. (2004). Estimation of observation impact using the NRL atmospheric variational data assimilation adjoint system. *Tellus A*, 56: 189–201.

Rosmond, T., and L. Xu, 2006. Development of NAVDAS-AR: Non-linear formulation and outer loop tests. Tellus A., 58, 45–58.

Stone, R.E., N. Baker, P. Pauley and B. Karpowicz, 2016. Comparison and Impact of Newly Available Atmospheric Motion Vectors in NAVGEM. *14th JCSDA Technical Review Meeting & Science Workshop on Satellite Data Assimilation*, Moss Landing, CA, Joint Center for Satellite Data Assimilation, Poster Session. [Available online at https://www.star.nesdis.noaa.gov/jcsda/meetings_Wkshp2016_posters.php].

Xu, L., T. Rosmond, and R. Daley, 2005. Development of NAVDAS-AR: Formulation and initial tests of the linear problem. *Tellus A*, 57, 546–559.

Global Forecast Dropout Prediction Tool in Support of the NCEP Model Evaluation Group (MEG)—Collaboration Project Between JCSDA/NESDIS & NWS

A project initiated between JCSDA/NESDIS and NCEP/EMC evaluates model forecasts through the NCEP Model Evaluation Group (MEG) focusing attention on the forecast system and real-time product-quality feedback into the model development cycle. The MEG evaluates the daily performance of NCEP forecast and analysis, identifies model biases, and conducts post-mortem studies of high-impact, poorly forecast events.

Poor forecasts or skill score *dropouts* occur in the National Weather Service (NWS) Global Forecast System (GFS) when other national center forecasts—for example, the European Centre for Medium-range Weather Forecasting (ECMWF)—often do not exhibit a similar loss in skill (Alpert et al., 2009a, Alpert et al., 2009b, Ballish et al., 2009, and Kumar et al., (2009, 2016)).

NCEP's current operational GFS model is a spectral T1534 (13 km) and includes a Gridpoint Statistical Interpolation (GSI) analysis for initializing the deterministic and other operational global and regional models. Recent upgrades have reduced Northern Hemisphere (NH) and Southern Hemisphere (SH)

(continued on page 6)

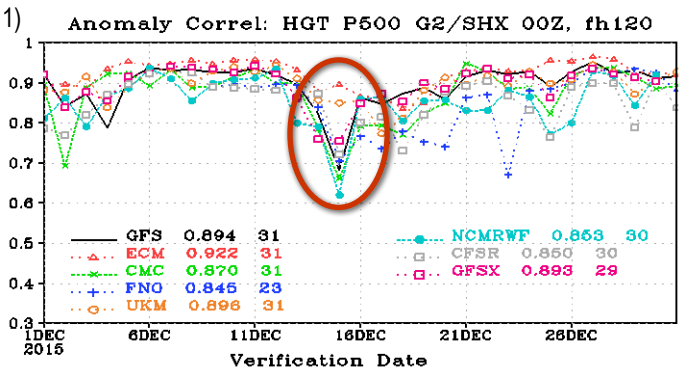

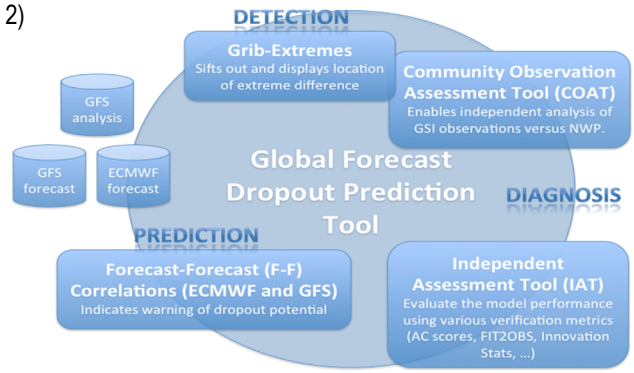

Figure 1. *Southern hemisphere 500-hPa geopotential height Anomaly Correlation time series for Dec. 1, 2015, to Dec. 31, 2015, for NCEP's operational GFS (black), parallel GFS (magenta rectangle), ECMWF (red triangle), UKMO (orange rhombus), CMC (green x), FNO (blue +), NCMRWF (cyan circle) and CFSR (gray rectangle). Marked red oval indicates a SH low-skill forecast AC score of ~0.7 and the parallel GFS AC score of ~0.75 for the operational and parallel GFS (http://www.emc.ncep.noaa.gov/gmb/STATS_vsdb/).*

Figure 2. *Components of the GFDPT.*

dropouts so they occur with less frequency and severity. The occurrence of GFS NH and SH forecast skill dropouts (percent 5-day Anomaly Correlations (AC) smaller than 0.7) shows a steady reduction from ~10–20 percent per year over the NH and ~30–40 percent per year over the SH during 1996–2001 to about 2–5 percent dropouts per year since 2007. This history of low forecast skill GFS dropouts from 1996 is archived in the NCEP at http://www.earthsystemcog.org/site_media/projects/gfsmodelingschool/nemsgfs_verif_fy.pptx.

Thus, the enhancements in the GFS model and GSI have reduced the occurrence and severity of GFS NH and SH forecast skill dropouts. However, dropouts continue to affect the GFS performance statistics compared to other international centers—e.g., ECMWF—and an investigation of how they can be alleviated is warranted. For example, Fig. 1 depicts the SH 5-day 500-hPa geopotential AC scores from December 1–31, 2015, at 00Z from multiple NWP centers. The marked red oval indicates a SH GFS dropout with an AC score of 0.68. ECMWF model forecast busts or dropouts, which occur less frequently than in the GFS, were also investigated by Rodwell et al. (2013) and Lillo and Parsons (2016).

In the past, an attempt to quantify model skill differences when there are dropouts was studied with the focus on quality control (QC) of conventional observations which were hypothesized as needing attention. Corrections to a number of observation types were accomplished—for example, correcting the position errors and bias and QC of aircraft and radiosonde (Ballish and Kumar, 2008; Zhu et al. 2015).

Global and regional area(s) were defined at initial condition (IC) time that had an impact on improving GFS 5-day forecasts when ECMWF analysis information was substituted. QC issues for conventional observations were investigated as the cause of dropouts in forecast skill, but no direct cause could be found for the low-skill event cases. However, there was some evidence that non-

(continued on page 7)

conventional observations could influence the 5-day forecast outcome in a few cases. This was found when only conventional data including RAOBS, ships, buoys, aircraft, and satellite cloud track winds were used to make a control IC, but not including radiance observations. Globally removing a single satellite radiance observation type showed little improvement, but for some dropouts a judicious selection of satellites could alleviate the dropout (Alpert et al., 2009a). If there were QC issues in a region with radiance contributions, removing all contributions would remove good information content even if there were issues with a fraction of the radiances.

The Global Forecast Dropout Prediction Tool project (GFDPT) goal is to detect, analyze, and improve QC by developing a monitoring system to analyze regional differences between the NCEP and ECMWF global models operationally and determine if the dropouts originate from QC problems in the assimilation, especially the assimilation of radiances. This study provides evidence as to what causes GFS dropouts, which continue to affect the GFS performance statistics, and how they can be alleviated.

GFDPT Components: Prediction, Detection, and Diagnosis of Forecast Dropouts

The various components of the GFDPT system are the prediction and detection of actionable volumes of conventional and satellite observations that cause the dropouts as illustrated in Fig 2. The *forecast-forecast* (F-F) correlations between ECMWF and GFS provide first warning of GFS dropout potential, an *extremes code* sifts out and displays extreme volumetric integrals of squared differences of geophysical fields of GFS analysis differences compared with ECMWF and other background guess fields, and finally a full diagnosis of actionable volumes is performed using the GSI diagnostics files. An independent *community observation assessment tool* (COAT) consisting of passive microwave, broadband, and hyper-spectral IR radiance measurements and atmospheric motion vectors indicates the extent that background is responsible for the dropout. NCEP's real-time data monitoring system (http://www.nco.ncep.noaa.gov/pmb/nwprod/realtime/) provides counts of conventional and satellite observations used by GDAS and GFS systems.

Regions in the IC that cause a dropout can be determined by vectoring at vertical levels, for example, the 5-day 500 hPa forecast error, back in time to the IC. Often multiple-source regions from a single 5-day forecast IC can occur. Once source regions are found that potentially were the cause of a dropout, a post-mortem experiment is carried out for GFS dropout cases using the ECMWF gridded analysis (1^{o}x1^{o} 14 standard pressure levels) made into pseudo observations for GSI input and GFS model forecast. These forecasts are called "ECM" runs and used to confirm if improvements in initial conditions to this source region, the proxy being ECMWF ICs, are applied and alleviate the dropout.

Whether dropouts originate due to model problems or assimilation issues cannot be definitively deduced, but this evidence can point to improvements in QC, as both assimilation and model issues are components in improving forecasts. We show preliminary evidence that contaminated radiances can potentially cause poor-skill GFS forecasts when they are assimilated in a region that is sensi-

(continued on page 8)

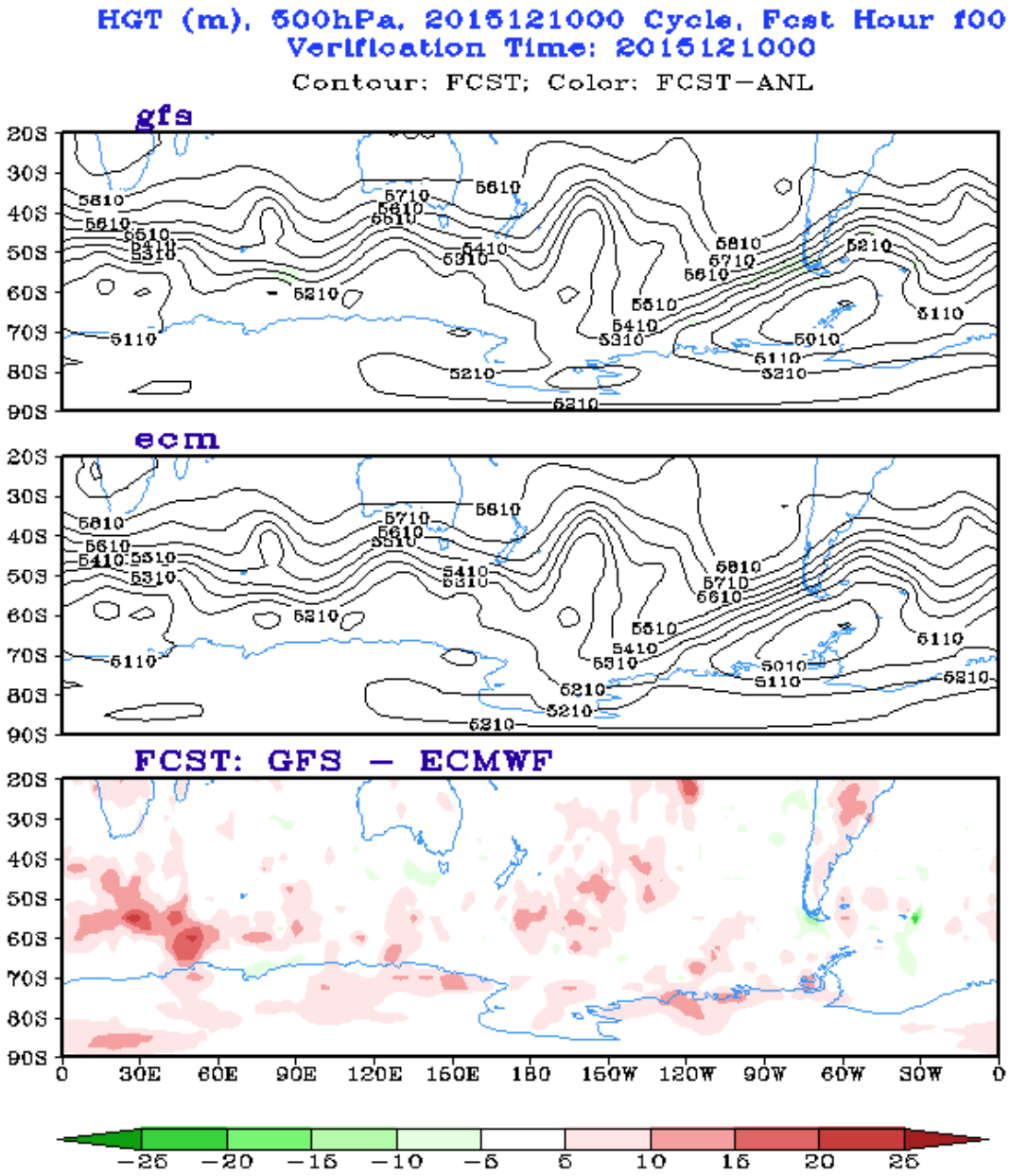

Figure 3. *GFS 500 hPa height and forecast error (top), ECMWF (ecm) 500mb height and forecast error (middle) and differences between GFS-ECMWF (bottom) at the IC time (f00) 2015121000Z over the SH. Colors indicate the forecast error.*

tive to IC in terms of the 5-day forecast error and indicate the extent that the background (model) is responsible for the dropout.

The GSI's "radstat" files contain radiance diagnostic information of the assimilated conventional and satellite observations such as the collocated observations, observation minus background (O-B), and observation minus analysis (O-A) fields which can be independently confirmed using the COAT. A web display of the GSI radiance statistics including the QC flags over a global domain with labels of extreme volumetric differences between GFS and ECMWF (Grib Extremes) as clickable points that display GSI diagnostics maps surrounding the extreme locations (Kumar et al. 2016) are an important aspect of relaying GFDPT information to forecasters.

(continued on page 9)

Case study of December 15, 2015, 00Z GFS SH dropout

The prediction and diagnosis components of the GFPDT are applied to the GFS 5-day dropout that occurred on December 15, 2015, 00Z over the SH (Fig. 1). Forecast error difference maps are used to compare the 500 hPa geopotential and at other vertical levels of the GFS and ECMWF at the IC time 20151210 at 00Z. Forecast errors appear amplified over troughs and ridges where there are high gradients in both GFS and ECMWF height fields (Fig. 3 GFS, top panel) and ECMWF (middle panel). SH GFS-ECMWF differences (Fig. 3 bottom panel) show a zonal structure and have high values particularly in the baroclinic zone. The GFS geopotential heights have higher values compared to ECMWF as shown by the red color fill in that area. Most of the SH forecast error at the IC time is located in a latitude band from 50ºS to 70ºS from three or four trough ridge pairs.

GSI Radiance Diagnostics and Discussion

The satellite radiance observations and the radiance calculated from the GSI production analysis using the forward model Community Radiative Transfer Model (CRTM) after bias correction are shown in Fig. 4 for AMSU-A Channel 1 O-A (top left) and ATMS-NPP Channel 1 (bottom left) at the IC 20151210 00Z. The large O-A (± 4 K) values observed over the swaths coincide with the baroclinic regions between 45ºS–70ºS of the SH. The potential errors in the radiance QC

(continued on page 10)

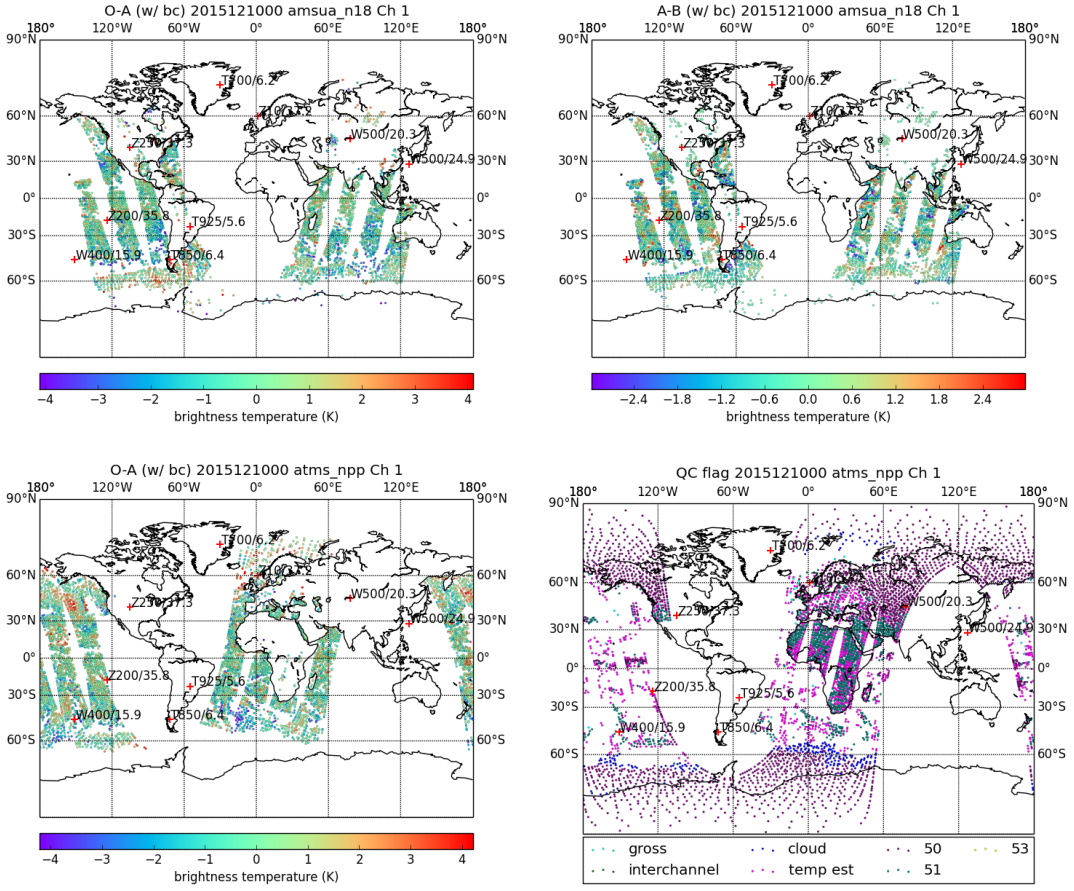

Figure 4. *GSI O-A after bias (top left) and A-B after bias correction at the IC 20151210 00Z for AMSUA-N18 Channel 1 (top right); GSI O-A after bias correction (bottom left) and GSI radiance QC flags distribution at the IC 20151210 00Z for ATMS-NPP Channel 1.*

analysis steps after the calculation of radiance observation departure can arise due to instrument problems, clouds and precipitation simulation errors, surface emissivity simulation errors, or wrong height assignment errors. Global satellite cloud pictures (not shown) at the IC 20151210 00Z show dense cloud—e.g., comma clouds—not unexpectedly in regions of large-amplitude trough-ridge containing multiple waves and high gradients of wind and height over the baroclinic regions in the SH. Therefore, contamination of observed radiance by clouds, precipitation, surface ice or other phenomena could potentially contribute to large O-A and A-B values (Fig. 4 top). Contaminated radiance could creep into the assimilation system, as evidenced by the voided areas of the GSI QC flags distribution that overlap the sensitive regions at the IC 20151210 00Z for ATMS-NPP Channel 1 (Fig. 4, bottom right). Red stars in Fig. 4 indicate the top five regions where extreme volumetric differences between GFS and ECMWF analyses are located from the Grib Extremes code.

GFS/ECM experiments and Observing System Experiments (OSE)

To address the question of whether the dropout is due to model problems or analysis problems, we use the GSI as a *Grand Interpolator*, with ECMWF pseudo-observations called "ECM" experiments generating a new IC that inherit ECMWF analysis characteristics. When GFS production analysis pseudo-observations are used as input constrained in the same way as above, the IC produces forecast skill similar to GFS production forecasts (Alpert et al. 2009). We target an ECMWF IC patch overlaid over GFS dropout source area(s) for a new IC that had impact on improving GFS 5-day forecasts. ECM experiments were carried out using the December 10, 2015, 00Z IC for the 5-day SH dropout that occurred on December 15, 2015, at 00Z in Fig 1.

GFS operations showed a 5-day dropout with 0.68 AC score; the ECM run improved the AC score to 0.87; and the ECMWF operations had an AC score of 0.90. An overlaid area run with the ECMWF ICs placed over the baroclinic zone (45°S-70°S), replacing the GFS production ICs in that area, which potentially caused a 0.68 AC score dropout, improved the AC skill score to 0.82. The overlaid experiment showed an AC score significantly higher than that from GFS production, representing the best the GFS could do if this source area had the information content from ECMWF. This experiment is typical and shows that ECM runs work remarkably well to alleviate the GFS operational dropouts. The ECM run output used in conjunction with other observations typically serves as a good post-mortem tool for diagnosing GFS model dropouts and to pose controlled IC experiments.

We performed a series of OSE experiments, fully cycled GSI (4DENSVAR Hybrid ENKF GDAS system) as in production (T1534) from 2015120718Z IC and GFS forecast to determine the sensitivity of high impact MW channels to show the cause of the SH December 15, 2015, 00Z dropout. In the experiment, PR4DEVSC (green), ATMS channels 1–5 and 15, and AMSUA and AMSUB channels 1–5 were denied over targeted patches identified by the GFS and ECMWF differences at the IC time. The lat-lon boxes (30°N–90°N, 140°E–240°E); (60°N–90°N, 300°–330°); (40°S–90°S, 0°E–160°E); (40°S–90°S, 180°E–300°E) were chosen to deny the surface channels over the above-mentioned

(continued on page 11)

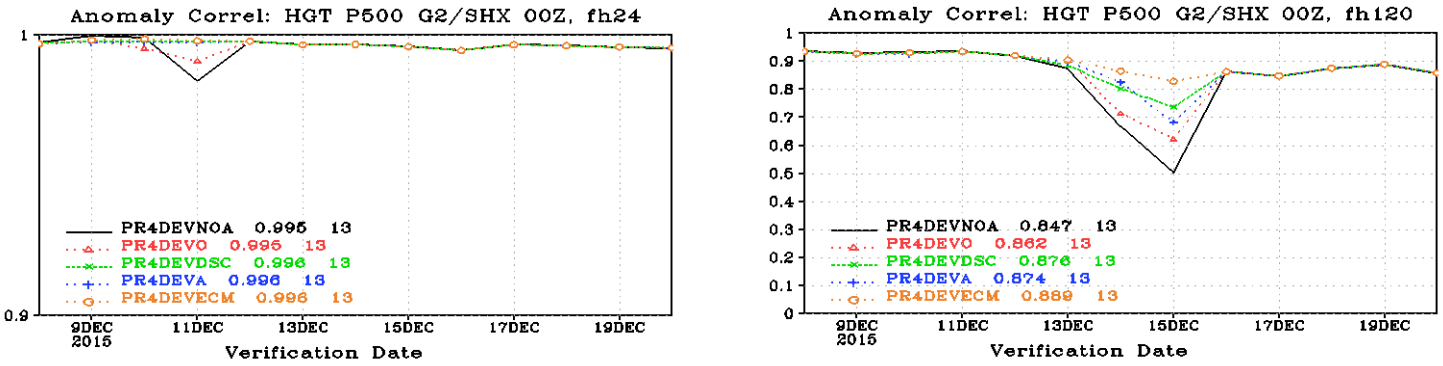

Figure 5. *AC of HGT Dec. 15, 2015 dropout between GFS (operations, PR4DEVA – blue), GFS using ECM IC (PR4DEVECM), PR4DEVDSC (OSE run denying MW surface channels – green), PR4DEVNOA (GFS run with no observations that started with the GDAS background – black), PR4DEVNO (GFS run with no observations as in PR4DEVNOA but started with the ECMWF analysis as background - red). Left panel is 1-day AC score and right panel is 5-day AC score.*

sensitive region. The experiment PR4DEVECM (Fig. 5, orange), shows the GFS run using ECMWF analysis (ECM run) as assimilated pseudo radiosonde data. The experiment PR4DEVDSC partially alleviated the SH dropout from AC score of 0.68 (GFS operations PR4DEVA in blue) to AC score of 0.75 at day 5 (PR4DEVDSC, green). The experiment PR4DEVECM improved the AC score significantly to 0.85 at day 5. In summary, removing the surface channel radiances from the analysis over dropout source areas caused improvement in the skill.

To understand the role of GDAS and ECMWF backgrounds, two experiments with no observations were performed (i) PR4DEVNOA (Fig. 5, black) initialized with the GDAS background and (ii) PR4DEVO (Fig. 5 red) initialized with the ECMWF analysis as background. In the background-only experiments, PR4DEVO and PR4DEVNOA, both show the AC skill signature of a dropout with a lead forecast time of 24 hours (Fig. 5 left panel, black) and resulting in a dropout at day 5 (Fig. 5 right panel, black). The dropout is significant for PR4DEVNOA (black), AC 0.5, with GDAS as background, and less so compared to PR4DEVO (red), AC 0.6, with the ECMWF analysis as background showing the dominant role of background and model errors. This finding was done for the equivalent of a 7-day forecast; eight cycling analysis and subsequent ECM forecast run leading up to the December 10 dropout. This illustrates the intricacies of isolating the initial and model errors and the role of background, dynamics, and physics of the GFS model in contributing to the accumulation of final errors. The background guess contribution (from model and physics) may also contribute but are intricate to separate. This one case study doth not a statistic make; therefore, more dropout experiments are required to confirm these statistics.

Summary and Future Work

We show there is evidence that contamination of observed radiance by cloudy, precipitating, surface ice or other phenomena could potentially contribute to large O-A and A-B values especially in ATMS lower tropospheric channels. While this effect probably happens globally and typically, we find it

(continued on page 12)

only in regions for ICs that result in a substantial dropout or low-skill score event in the GFS. Dropout source regions ICs that replace the GFS with ECMWF ICs alleviate the dropout regardless of the background. The large GSI weights and global density attributed to pseudo observations (used as RAOB type) may overwhelm the background compared with the time it takes radiance changes to influence the forecast. In addition, using the equivalent of a 7-day forecast of the dropout, it was found that by adding no observations to the background for controlled (1x1 degree and 14 layer) IC experiments, the influence of the background was about a third of that to assimilating (pseudo) observations. This was done for the equivalent of a 7-day (dropout) forecast, so this ratio is liable to change when one uses a 5-day or shorter forecast length.

Future investigations will focus on understanding the cycle-to-cycle variance of radiance data from high-impact satellite channels and using this information to improve the production QC. Therefore, one can improve forecasts not only by improving QC by modification and filtering out contaminated observations, but also by utilizing new information such as that from observation sources fused to make background adjustments a priori.

In addition, when dropouts occur there will be interaction with WPC forecasters and the MEG reminiscent of "Tiger teams" with GDPFT tools to react to low-skill forecast events perhaps as soon as the next cycle, with a goal of a permanent QC solution.

V. Krishna Kumar, Andrew Eichmann (RTi at NOAA/NESDIS/JCSDA), Jordan Alpert (NOAA/NCEP/EMC), and Sid Boukabara (NOAA/NESDIS/STAR)

References

Alpert, J.C., D.L. Carlis, B.A. Ballish, and V.K. Kumar, 2009a. Using "pseudo" RAOB observations to study GFS skill score dropouts. *23rd AMS Conference on WAF* https://ams.confex.com/ams/23WAF19NWP/webprogram/Paper154268.html

Alpert, J.C., D.L. Carlis, B.A. Ballish, and V.K. Kumar, 2009b. Improved forecast skill using pseudo-observations in the NCEP GFS. *13th AMS IOAS-AOLS*, P2.1. https://ams.confex.com/ams/89annual/techprogram/paper_142649.htm

Ballish, B.A., J. Alpert, D. Carlis, and V.K. Kumar, 2009. What Causes NCEP GFS Model Forecast Skill "Dropouts", *13th AMS IOAS-AOLS*, 2.1 https://ams.confex.com/ams/89annual/techprogram/paper_142644.htm

Ballish, B.A, and V.K. Kumar, 2008. Systematic differences in aircraft and radiosonde temperatures: Implications for NWP and climate studies. *Bull. Amer. Meteor. Soc.*, 89 (11), 1689–1708 DOI: http://dx.doi.org/10.1175/2008BAMS2332.1

Kumar, V.K., J.C. Alpert, D.L. Carlis, and B.A. Ballish, 2009. Investigation of NCEP GFS model forecast skill "dropout" characteristics using the EBI index. *23rd AMS Conference on WAF* https://ams.confex.com/ams/23WAF19NWP/techprogram/paper_154282.htm

Kumar, V.K., E. Maddy, J.C. Alpert, and S.A. Boukabara, 2016. Global forecast dropout prediction tool in support of the NCEP model evaluation group (MEG)—A collaborative project between JCSDA/NESDIS & NWS.

(continued on page 13)

20th AMS Conference IOAS. https://ams.confex.com/ams/96Annual/webprogram/Paper288630.html.

Lillo, S.P., and D.B. Parsons, 2016. Investigating the dynamics of error growth in ecmwf medium range forecast busts. Quarterly Journal of the Royal Meteorological Society: n/a–n/adoi:10.1002/qj.2938, URL http://dx.doi.org/10.1002/qj.2938. QJ-15-0196.R2.

Rodwell, M.J., L. Magnusson, P. Bauer, P. Bechtold, M. Bonavita, C. Cardinali, M. Diamantakis, P. Earnshaw, A. Garcia-Mendez, L. Isaksen, E. Källén, D. Klocke, P. Lopez, T. McNally, A. Persson, F. Prates, and N. Wedi, 2013. Characteristics of occasional poor medium-range weather forecasts for Europe. *Bull. Amer. Meteor. Soc.* 94: 1393–1405.

Zhu Y., J.C. Derber, R.J. Purser, B.A. Ballish and J. Whiting, 2015. Variational correction of aircraft temperature bias in the NCEP's GSI analysis system. *Mon. Wea. Rev.* 143, 3774–3803, DOI: 10.1175/MWR-D-14-00235.1.

Latest Progress of All-Sky Microwave Radiance Assimilation in the GSI and the CRTM at NCEP

In the past decade, with the advances of forecast models including their physics and the improvement of radiative transfer models, numerical weather prediction (NWP) centers have made steady progress toward utilizing cloudy radiances as well as radiance observations in clear sky. The European Centre for Medium-Range Weather Forecasts (ECMWF) achieved direct all-sky radiance assimilation for the Special Sensor Microwave/Imager (SSM/I) and the Advanced Microwave Scanning Radiometer for Earth Observing System (AMSR-E) in 2009 (Bauer et al. 2010; Geer et al. 2010). Comprehensive studies have also been conducted in other NWP centers, such as Met Office and Japanese Meteorological Agency.

Capability for all-sky microwave radiance assimilation in the Gridpoint Statistical Interpolation (GSI) analysis system has been developed at the National Centers for Environmental Prediction (NCEP), and the assimilation of cloudy radiances from the Advanced Microwave Sounding Unit-A (AMSU-A) microwave radiometer for ocean fields of view (FOVs) became operational in the Global Forecast System (GFS) on May 12, 2016 (Zhu et al. 2016) as the GFS was upgraded to the 4D hybrid Ensemble-Variational (EnVar) system. The assimilation of cloudy AMSU-A radiances in the GFS improves the temperature and relative humidity off the west of the continents as well as reducing a known positive bias of stratus.

Since the implementation of all-sky radiance assimilation of AMSU-A in the GFS, significant progress has been made in the all-sky GSI. To facilitate the expansion of the all-sky approach to additional microwave and infrared sensors, the GSI codes for the all-sky capability are generalized with all-sky sensor selection specified in the sensor

(continued on page 14)

information table. The all-sky related procedures, which were scattered in various parts of the GSI and for different sensors, are now controlled by a centralized module and data structure along with a fixed file of all-sky parameters. Moreover, the all-sky approach is being expanded to radiances of Advanced Technology Microwave Sounder (ATMS).

Two other efforts are also under development for the general enhancement for all-sky radiance assimilation. One is the application of the new variational quality control scheme (VQC, Purser 2011) to radiance data, and the other is the treatment of subgrid-scale convective clouds in the GSI. Meanwhile, in the CRTM, fractional cloud coverage (Geer and Bauer 2009) was developed, and a bug in scattering calculation was fixed.

In this article, we briefly describe the current configuration of the GSI all-sky radiance assimilation, followed by a description of ongoing work in the GSI and the CRTM in more details, and finally future work and plan.

The GSI all-sky radiance assimilation capability involves considerations of several aspects, and detailed information can be found in Zhu et al. (2016). While the all-sky GSI has the flexibility to choose either normalized cloud water or individual hydrometeors (cloud liquid water, cloud ice, snow, rain, graupel, hail) as the cloud control variable(s), normalized cloud water is currently used for the GFS system as cloud water is the prognostic variable in its forecast model.

In the 4D EnVar framework, background error covariance is composed of the static term and ensemble contributions. For the ensemble part, the cloud background error variance and covariances with other variables are extracted implicitly from the ensemble perturbations, but covariances between cloud and other variables are not specified in the static term yet. Observation error assignment is based on the symmetric observation error method (Geer and Bauer 2011) and situation-dependent observation error inflation. For the bias correction (Zhu et al. 2014a,b), only a selected data sample, where clouds retrieved from the observation and those from the first guess are consistent, are used to derive the bias correction coefficients, and then these coefficients are applied to all radiance data.

Currently, only the radiances affected by non-precipitating clouds are assimilated in the GFS due to the lack of precipitation and snow information in the model forecast output. Quality control procedures include surface emissivity sensitivity check, cloud effect check, precipitation screening, and gross error check. In the GFS forecast model, the moist physics schemes consist of the cloud microphysics parameterization (Zhao and Carr 1997, Sundqvist et al. 1989, Moorthi et al. 2001) and parameterizations of deep and shallow cumulus convection (Han and Pan 2011).

To further enhance and expand all-sky radiance assimilation, there are several ongoing development efforts in the GSI. One of them is the expansion of all-sky radiance assimilation to ATMS. ATMS has 22 channels, combining most of the channels from AMSU-A and Microwave Humidity Sounder (MHS). ATMS is different from AMSU-A and MHS in beam width, number of field of views, and scan swath width. Some channels also have different frequency/polarization. In this study, all-sky AMSU-A quality control procedures are adopted for ATMS, but ATMS radiances over

(continued on page 15)

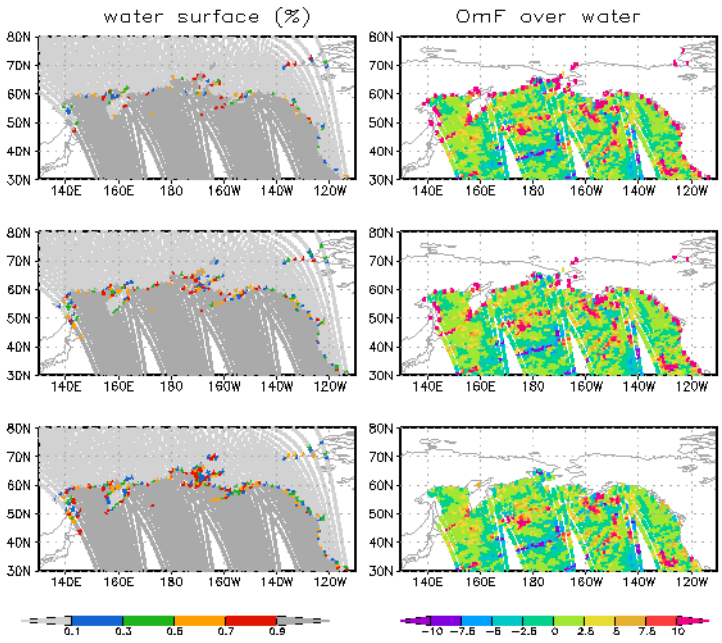

Figure 1. *Water surface percentage (left) and OmF (K) over water for ATMS channel 2 (right) with different FOV configurations: interpolation using the four nearest grid points (top), FOV relative antenna power at edge decreasing to 50 percent (middle) and 1 percent (bottom).*

ice, snow, and mixed surfaces are not used. Efforts have been focused on the additional procedures due to unique ATMS features.

Unlike AMSU-A, ATMS has varied beam widths, 5.2 degrees for channels 1 and 2, 2.2 degrees for channels 3-16, and 1.1 degrees for channels 17–22. In the current operational clear-sky ATMS radiance assimilation, the ATOVS and AVHRR Pre-processing Package (AAPP, NWP SAF/EUMETSAT) spatial averaging is applied to only channels 1–16 to convert the beam widths to 3.3 degrees. In this all-sky ATMS study, the spatial averaging is applied to all channels of ATMS. This facilitates the application of a common beam width of 3.3 degrees for all ATMS channels in calculating FOV and cloud amount/detection.

Moreover, in the operational clear-sky ATMS radiance assimilation, the surface properties (including land and sea distribution) at observation locations are calculated as interpolations using the four nearest model surface grid points. This is not appropriate given the T1534/T574 resolution of the GFS 4D EnVar system and the size of the FOV. The capability of modeling surface properties based on the FOV size and shape is activated for the all-sky ATMS radiances. The impact of FOV size/shape on the surface property calculation and quality control are investigated, especially for the radiances with a large departure from the first guess (OmF) around coastlines and cryosphere boundaries.

The left column of Fig. 1 shows the water surface percentage (%) when surface type is calculated as interpolation using the four nearest model surface grid points (left top) and with FOV calculation where the relative antenna power at the FOV edge decreases to 50 percent (left middle) and 1 percent (left bottom) of the maximum at the center. Dark gray color points represent the water-surface type locations, and colored points the mixed-surface type locations. As expected, more observation locations are marked as mixed-surface type around the

(continued on page 16)

coastline when the FOV antenna power at the edge decreases to 1 percent.

Although ATMS radiances with large OmFs are found around the coastline in all three configurations, the quality control procedure of excluding data over mixed-surface type makes the difference. The corresponding brightness temperature (TB) OmFs over water are displayed in the right column for ATMS channel 2. As the observations with large OmFs around the coastline pass the quality control when interpolation with the nearest four model grid points is used for surface property calculation (right top) and when FOV antenna power at edge decreases to 50 percent (right middle), it is seen that these observations are excluded effectively from the system when FOV antenna power at edge decreases to 1 percent (right bottom).

Additionally, the difference of cloud effects on channels 16 and 17 (88.2GHz and 165.5GHz), which are sensitive to ice clouds, is calculated as a scattering measurement, i.e., scattering=cloud_effect(ch16) – cloud_effect(ch17), where cloud_effect=TB_{cloudy} - $TB_{clear\text{-}sky}$. Observations from channels 1–7 and 16–22 are excluded if ($|scattering| > 20.0$). In this study, the ATMS-specific observation error is assigned as a function of cloud liquid water following the OmFs' behavior, and the all-sky cycling ATMS radiance impact experiments are underway.

The effort on the application of new VQC (Purser 2011) to radiance data is also ongoing. In the GSI, radiance observation error distribution is assumed to be Gaussian. However, in the all-sky approach, many useful cloudy radiances are associated with large OmFs and of non-Gaussian distribution. Currently, the situation-dependent observation error inflation has been applied to the radiances with large OmFs, so these data can still be used in the analysis with reduced weights while not shocking the system. Since VQC (Andersson and Jarvinen, 1998; Tavolato and Isaksen 2014; etc.) accounts for the non-Gaussian nature of gross measurement errors in its formulation, it is expected that the application of VQC can serve our purpose.

The original VQC formulation, a linear combination of Gaussian and flat distributions, has been applied to only conventional data in the GSI. However, this non-Gaussian distribution may lead to multiple-minima in the cost function. A new probability model for representing realistic measurement errors (Purser 2011), which generalizes the "logistic" distribution, ensures that the negative-log-posterior distribution preserves the property of convexity possessed by the negative-log-prior, and is therefore free of multiple minima. Fig. 2 displays the logarithm of normalized OmF histogram (black dots) for AMSU-A NOAA18 during the period from June 1 to July 20, 2015. The green curve represents Gaussian distribution $f(x)=\exp[-(x-m)^2/(2s^2)]$, and the red curve Logistic distribution $f(x)=\mathrm{sech}^2[(x-m)/(2s)]$. The parameters of the Gaussian and Logistic distributions are estimated using entropy fitting to the OmFs.

It is seen that channels 1–5 and 15 resemble logistic distribution while channels 7–10's patterns are quite Gaussian. The generalized logistic distribution $f(x)=\exp^{abx}\ \mathrm{sech}^{2b}[(x-m)/(2bs)]$ derived in Purser (2011) can be used for both scenarios with different estimated parameters. As b increases, the generalized logistic distribution becomes more Gaussian. Preliminary results of the

(continued on page 17)

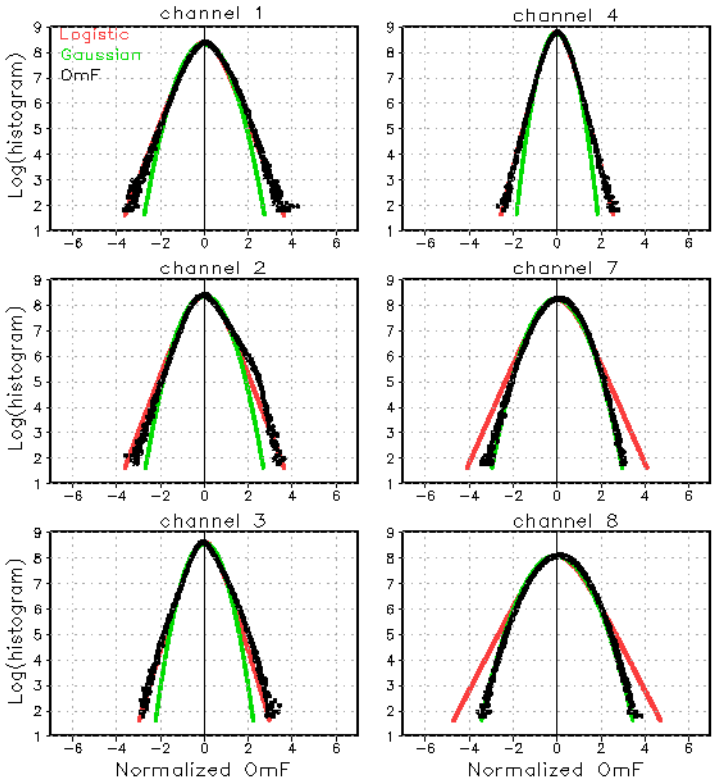

Figure 2. *Logarithm of normalized OmF histogram (black dots) for AMSU-A NOAA18, and curves of Gaussian (green) and Logistic (red) distributions.*

cycling experiments indicate that this new VQC could replace the situation-dependent observation inflation that is currently used on all-sky radiances. More refinement of the VQC algorithm and tuning continues.

Another effort on further improving the all-sky radiance assimilation is the treatment of convective clouds in the GSI. Convective parameterization schemes are usually used in global models, though some regional nest domains don't use them. In the GFS, clouds due to convection are only considered through detraining the convective cloud water to the grid scale cloud water near the convective cloud tops; thus, the cloud condensate in the convective plume is not included in the total condensate of the forecast model output, and these subgrid-scale convective clouds currently are not available for use in the GSI.

We need to handle these subgrid-scale clouds in the GSI correctly, as the radiance observations contain the information of convective clouds. The lack of convective clouds will affect not only the simulated radiances but also the ensemble spread of clouds, and subsequently the analysis increments, especially for the lower model levels of the tropics. On the other hand, although the convective clouds need to be taken into account in the radiance data assimilation, the subgrid-scale clouds should not be included in the generated cloud analyses nor fed back to the model forecast. Different strategies with additional convective cloud control variable(s) and/or model physics are being explored.

As the enhancement efforts are in progress in the GSI, new development and bug fix were also made in the CRTM. In current NCEP operational GFS, the cloud-affected AMSU-A radiances are assimilated under the assumption that the cloudy columns

(continued on page 18)

are overcast. In other words, the total cloud cover as viewed by satellite sensor is always one. This is due to two practical reasons: the CRTM does not handle fractional clouds, and the GFS forecast output does not provide cloud fraction profile to GSI. This is problematic in simulating brightness temperature for sensor field of view with small-scale variability of cloud and precipitation.

At microwave frequencies, the non-linear effect of radiance on hydrometeor amount causes a "beam-filling effect" in satellite observation (Kummerow 1998). Even when two fields of view contain the same mass of hydrometeors, variations in fractional cloud coverage can result in large differences in observed radiances. To better handle the fractional cloudiness conditions, CRTM has enhanced its all-sky capability by implementing various cloud overlap schemes to estimate the total cloud cover and the two-columns radiance calculation to account for partially cloudy scenes (van Delst et al., 2016). The viewing column is split into two parts: clear and cloudy sub-columns. The all-sky brightness temperature which depends on the total cloud cover C_{total} is calculated as follows: $TB_{allsky} = (1\text{-}C_{total}) \times TB_{clear} + C_{total} \times TB_{cloudy}$, where TB_{clear} and TB_{cloudy} are the brightness temperatures for the clear and cloudy sub-columns, respectively. Three commonly used cloud overlap schemes: maximum, random, and maximum random schemes (Hogan and Illingworth, 2000) had been developed in CRTM and they are calculated based on the user input of cloud fraction at each model layer. In addition, the hydrometeor-weighted cloud cover scheme (averaged scheme) was also implemented following the method proposed by Geer and Bauer (2009) for microwave radiative transfer, in which the total cloud cover is an average cloud fraction over the whole profile, weighting by the total hydrometeor amount. The impact of the fractional clouds on simulated brightness temperature is larger in high frequency channels. As shown in Fig. 3a for 89 GHz AMSU-A using the averaged method, the difference in brightness temperature can be as large as 30 to 50 degrees at rainy and snowy locations. The impact of total cloud cover estimated from various cloud overlap schemes on brightness temperatures are shown in Fig. 3b for IASI 616 channel set. As expected, the greatest impact can be found at window channels, and the random overlap scheme gives the largest impact, whereas the averaged scheme has the smallest effect on calculated brightness temperature. It should be noted that while the averaged scheme is a more appropriate

(continued on page 19)

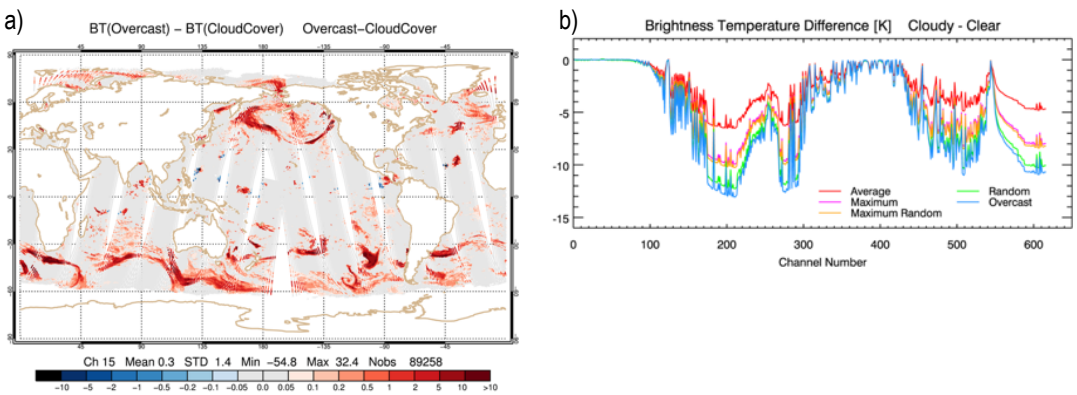

Figure 3. *Impact of fractional clouds on CRTM simulated brightness temperatures for: (a) AMSU-A and (b) IASI.*

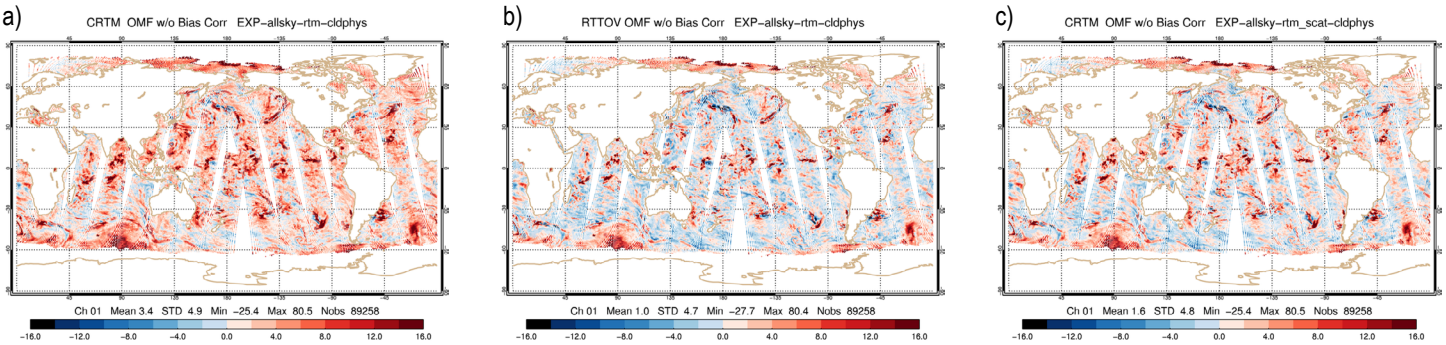

Figure 4. *Observed minus simulated brightness temperatures from: (a) CRTM without the work-around, (b) CRTM with the work-around, and (c) RTTOV for AMSU-A.*

method for estimating the total cloud cover for microwave sensors since clouds are more transparent to microwave radiation, the maximum-random scheme is probably more appropriate for infrared sensors. The assessment of the impact of cloud fraction on microwave and Infrared sensors on analysis and forecast are currently underway.

To prepare for the assimilation of microwave radiances affected by rain and snow, an experimental GFS with precipitation (rain and snow) output was used to investigate the scattering radiative transfer at microwave frequencies. It was found that the calculated brightness temperatures from CRTM have systematic biases for surface-sensitive channels at locations where the ADA solver is involved as compared to those calculated from RTTOV (Figs. 4a and 4b). Further investigation revealed that the off-diagonal terms of the surface reflectivity matrix is zero so that no diffuse radiation is reflected towards the view direction.

Owing to the lack of proper surface reflectivity matrix for multiple-scattering radiative transfer, a work-around has been developed to reduce the biases: (1) reflection correction is included in conjunction with ADA solver and the correction is only applied to stream angles less than 60 degrees, (2) stream angles greater than 60 degrees are taken as 60 degrees when multiple scattering is on. The calculated brightness temperatures with the work-around indicate the biases are greatly reduced as compared to the observation, and they are also comparable those calculated from RTTOV (Figure 4c and 4b). The new development in total cloud cover and two-column radiance calculations to handle fractional cloudy scene and the inclusion of the modified reflection correction for radiation transfer under scattering condition will be incorporated into the incoming CRTM release (Rel-2.3.0).

As the forecast models are transitioning to FV3 and more advanced physics at NCEP, we will focus on adapting the all-sky radiance assimilation in the FV3 framework, and examine and re-tune the all-sky radiance assimilation with individual hydrometeors as cloud control variables should they later become the prognostic variables in the forecast model. As further refinements of all-sky assimilation continue along with the enhancements of the CRTM, all-sky radiance assimilation should be expanded to additional instruments and performed for radiances over land. Another aspect that still needs more attention is the choice of the cloud control variable(s). Al-

(continued on page 20)

though the current cloud control variable works reasonably well, we believe investigation of better cloud control variable(s) in the future will be beneficial, especially when combined with the consideration of balance among temperature, moisture, and clouds.

Yanqiu Zhu, Emily Liu, Paul van Delst, George Gayno, Jim Purser, Xiujuan Su (I.M. Systems Group at NOAA/NCEP/EMC, College Park, MD)

Acknowledgements:
We would like to thank our EMC colleagues, including: Ruiyu Sun, Jongil Han, John Derber, Brad Ferrier, Fanglin Yang, Li Bi, Andrew Collard, Dave Groff, Runhua Yang, Jun Wang and Xu Li for their helpful discussions.

References:

Andersson, E., and H. Jarvinen, 1998. Variational quality control. *ECMWF Tech. Memo*, 250, Reading, UK.

Bauer, P., A.J. Geer, P. Lopez, D. Salmond, 2010. Direct 4D-Var assimilation of all-sky radiances. Part I: implementation. *Quart J. Roy. Meteor. Soc.*, 136, 1868–1885.

Geer, A.J., P. Bauer, P. Lopez, 2010. Direct 4D-Var assimilation of all-sky radiances. Part II: Assessment. *Quart. J. Roy. Meteor. Soc.*, 136, 1886–1905.

Geer, A.J. and P. Bauer, 2009. A revised cloud overlap scheme for fast microwave radiance transfer in rain and cloud. *J. Applied Meteor. & Climat.*, 48, 2257–2270.

Han, J. and H.L. Pan, 2011. Revision of convection and vertical diffusion schemes in the NCEP Global Forecast System. *Weather and Forecasting*, 26, 520–533.

Hogan, R.J., and Illingworth, A.J., 2000. Deriving cloud overlap statistics from radar. *Quart. J. Roy. Meteor. Soc.*, 128, 2903–2909.

Kummerow, C., 1998. Beamfilling errors in passive microwave rainfall retrievals. *J. Appl, Meteor.*, 37, 356-370.

Liu, E.H., A. Collard, R. Sun., Y. Zhu, P. van Delst, D. Groff, J. Derber, 2015. Intercomparison of CRTM and RTTOV in NCEP Global Model. Available online at https://cimss.ssec.wisc.edu/itwg/itsc/itsc20/papers/8p_01_liu_paper.pdf.

Moorthi, S., H.L. Pan, P. Caplan, 2001. Changes to the 2001 NCEP operational MRF AVN global analysis/forecast system. *NWS Technical Procedures Bulletin 484*, available online at http://www.nws.noaa.gov/om/tpb/484.htm, 14.

Purser, R.J., 2011. Mathematical principles of the construction and characterization of a parameterized family of Gaussian mixture distributions suitable to serve as models for the probability distributions of measurement errors in nonlinear quality control. *NOAA/NCEP Office Note 468*, 42.

Sundqvist, H., E. Berge, J.E. Kristjansson, 1989. Condensation and cloud parameterization studies with mesoscale numerical weather prediction model. *Mon. Wea. Rev.*, 117,1641–1657.

Tavolato, C., and L. Isaksen, 2014. On the use of a Huber norm for observation quality control in the ECMWF 4D-Var. *ECMWF Tech. Memo.* 744, Reading, UK.

Van Delst P., E.H. Liu, L. Bi, 2016. Cloud fraction in the CRTM. *JCSDA Office Note CRTM-4*, rev71147, 36 pp.

(continued on page 21)

Zhao, Q., and F.H. Carr, 1997. A prognostic cloud scheme for operational NWP models. *Mon. Weather. Rev.*, 125, 1931–1953.

Zhu, Y., J. Derber, A. Collard, D. Dee, R. Treadon, G. Gayno, J.A. Jung, 2014a. Enhanced radiance bias correction in the National Centers for Environmental Prediction's Gridpoint Statistical Interpolation Data Assimilation System. *Quart. J. Roy. Meteor. Soc.*, 140, 1479–1492.

Zhu, Y., J. Derber, A. Collard, D. Dee, R. Treadon, G. Gayno, J. Jung, D. Groff, Q. Liu, P. van Delst, E. H. Liu, D. Kleist, 2014b. Variational bias correction in the NCEP's data assimilation system. *The 19th International TOVS Study Conference*, available online at http://cimss.ssec.wisc.edu/itwg/itsc/itsc19/program/papers/10_02_zhu.pdf, Jeju Island, South Korea.

Zhu, Y., E.H. Liu, R. Mahajan, C. Thomas, D. Groff, P. v. Delst, A. Collard, D. Kleist, R. Treadon, J. Derber, 2016. All-Sky Microwave Radiance Assimilation in NCEP's GSI Analysis System. *Mon. Weather Rev.*, 144, 4709–4735.

DEVELOPMENT EFFORTS

Addendum of 'CRTM Development Status and New Features in the Next Release' in JCSDA Quarterly No. 54, Winter 2017

This addendum provides additional information to clarify the discussion of the Community Radiative Transfer Model (CRTM) – Optimal Spectral Sampling (OSS) unapodized radiance simulations in the above article.

In the article, it was not mentioned explicitly that the CRTM – Optical Depth in Pressure Space (ODPS) apodized simulations were compared with the CRTM-OSS unapodized simulations and the Cross Track Infrared Sounder (CrIS) Sensor Data Record (SDR) unapodized observations. This comparison is misleading. The CRTM-ODPS method is

(continued on page 22)

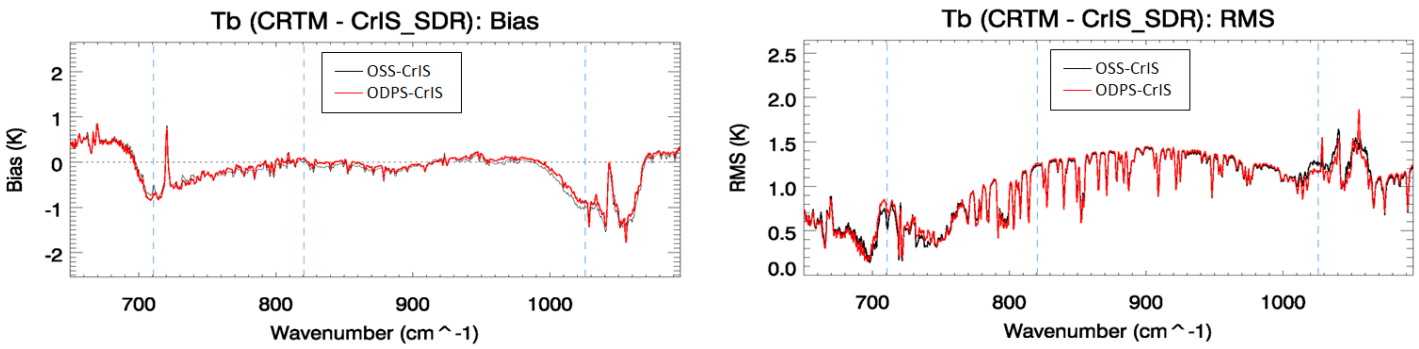

Figure 1. *The biases (a) and root mean square errors (b) of CRTM-OSS (black curve) and CRTM-ODPS (red curve) simulated apodized brightness temperatures as compared with CrIS SDR apodized observations under clear sky condition over ocean on 0600 UTC, March 29, 2016.*

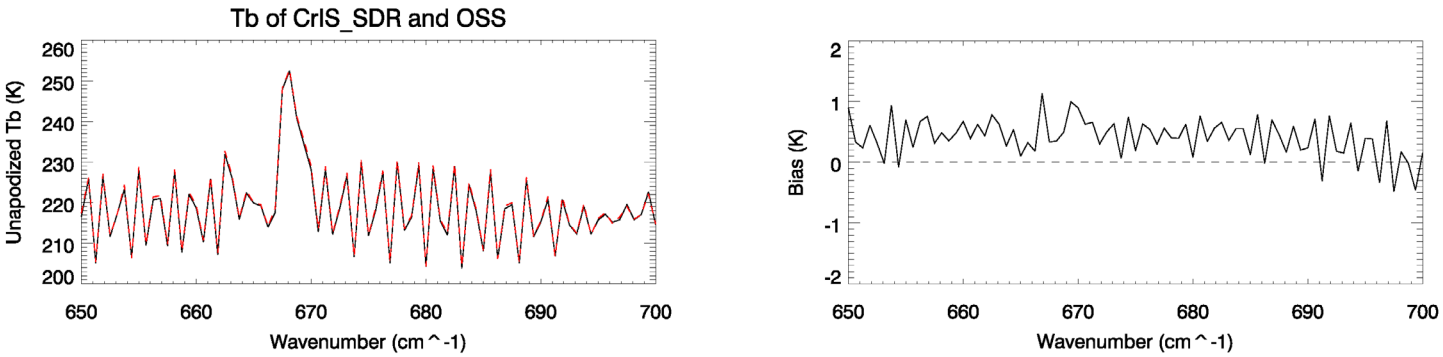

Figure 2. *The CrIS brightness temperatures from simulations and observations (a), and biases between the unapodized CRTM-OSS simulation (red dashed line) and the CrIS SDR unapodized observations (black solid line) (b) for the same profiles as that used in Fig.1 on 0600 UTC, March 29, 2016.*

designed for apodized radiance simulation, and in the current Gridpoint Statistical Interpolation (GSI) data assimilation system, the CrIS apodized radiance observation is used. If we also convert the CRTM-OSS simulation into apodized radiance, the comparison of these three radiances is given in Fig. 1. It can be found that the bias and RMSE from OSS and ODPS are comparable over ocean under a clear-sky condition. To demonstrate the radiance from OSS simulation capability of OSS method, we compare the CrIS unapodized radiances from OSS simulation with observations. As shown in Fig. 2, the bias between simulations and observations is generally within 1K in the CrIS longwave CO2 region.

Tong Zhu (CIRA/Colorado State University, Fort Collins, CO)

Unsolicited articles for the JCSDA Quarterly Newsletter are encouraged as are suggestions for seminar speakers or topics. Please send them to Biljana Orescanin, biljana.orescanin@noaa.gov.

OTHER NEWS

The Fifth AMS Symposium on the Joint Center for Satellite Data Assimilation (JCSDA)

The Symposium, chaired by Dr. Jim Yoe of the National Centers for Environmental Prediction (NCEP), was held as part of the 97th Annual Meeting of the American Meteorological Society in Seattle, Washington. The symposium was organized into 4 topical sessions featuring a total of 21 oral presentations, as well as 16 posters. Presentations were made by JCSDA partner agency personnel, the academic community, and by international representatives from as far away as Korea and Australia. All of the sessions were well attended, with audiences of 50 to 75.

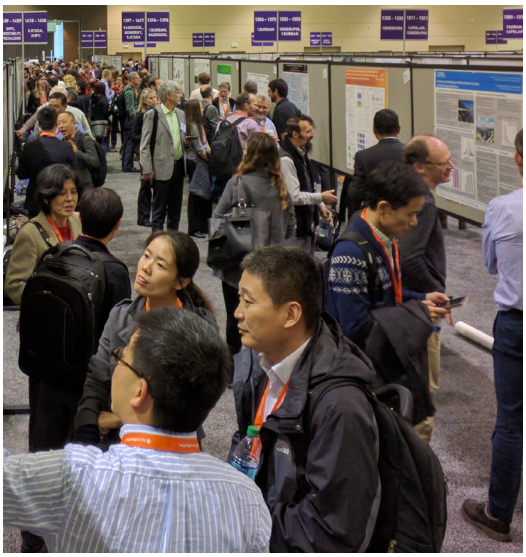

The opening session was co-chaired by Mike Ek (NWS/NCEP) and Nancy Baker (NRL) and featured five papers devoted to the assimilation of satellite data to improve analyses and forecasts of land surfaces (through the validation of FASTEM) and of air quality and aerosols in four different operational modeling systems. The second session featured six more presentations of assessments of data impacts on numerical weather prediction (NWP) skill, and was moderated by Fuzhong Weng (NESDIS/STAR) and Will McCarty (NASA/GMAO). The third session, chaired by Ron Gelaro (NASA/GMAO) and Ben Johnson (UCAR/JCSDA) featured three papers on quite varied topics, including developments in the CRTM to support Observation System Simulation Experiments for a Cubesat microwave sounder and other sensors, the development of an observation-based model skill "dropout" tool for potential use by NOAA's Model Evaluation Group, and variational control for all-sky radiance assimilation. The fourth and final oral session was chaired by former JCSDA Director John LeMarshall (Australian BOM) and Jim Yoe (JCSDA and NCEP) and comprised six contributions describing innovative methods for assimilating satellite observations. These included improved bias corrections for CrIS and microwave sounders, techniques for assimilating all-sky radiances, and accounting for correlated errors in the GSI.

The symposium co-hosted the 2017 Student Reception in Satellite Meteorology on the evening of Monday, January 23, and drew a number of young, mid-career, and senior-level scientists and professionals who took part in a very successful and popular Speed Mentoring exercise that allowed students to meet and ask questions. The Sixth AMS Symposium on the JCSDA is currently being organized for the 98th Annual Meeting of the AMS in Austin, TX, in January 2018.

PEOPLE

Welcome Dr. Yannick Trémolet

Dr. Yannick Trémolet joined the JCSDA in Boulder in January 2017. He will lead the Joint Effort for Data assimilation Integration (JEDI). The main objective of the project will be to define and implement the next-generation unified data assimilation framework for all JCSDA partners and the wider community. This framework will accommodate both operational and research needs through the use of modern software development techniques and tools. It will provide the infrastructure for exploring and addressing the grand scientific challenges for tomorrow's data assimilation and forecasting.

Yannick has a Ph.D. in Applied Mathematics and long experience in data assimilation and high performance computing (HPC). Before joining the JCSDA, he worked at the European Centre for Medium-range Weather Forecasts (ECMWF). His main research interests are in data assimilation methodology. More specifically, he has worked on the estimation of model error in weak constraint 4D-Var, on the use of long assimilation windows, on the convergence of 4D-Var, and on the scalability and efficiency of variational data assimilation. He initiated and led the implementation of the Object-Oriented Prediction System (OOPS) that aims at making the ECMWF data assimilation system more flexible for exploring new algorithms and more scalable.

Dr. Trémolet also spent one year at NASA/GMAO, where he worked on the implementation of 4D-Var in the GSI and implemented an adjoint of the assimilation system for observation impact estimation. Before joining ECMWF, he spent several years at NCEP/EMC, working mostly of the parallelization and efficiency of the global spectral model. He also developed the tangent linear and adjoint of that model.

Apart from science, Yannick enjoys travels, mountains and nature, often combining those through long treks in the Himalayas, the Andes, or the Arctic. He also enjoys skiing, photography, and cooking. He is very keen to start exploring the mountains around Boulder.

CAREER OPPORTUNITIES

An opportunity with AER for a satellite data assimilation scientist to support the NOAA-NESDIS activities in cloud-, rain- and ice- impacted radiance data assimilation in operational Numerical Weather Prediction (NWP) models is available.
The job posting:
https://careers.verisk.com/viewjob.html;jsessionid=93C56AB94DB813DB736A161D22B7B08D?optlink-view=view-49836&ERFormID=newjoblist&ERFor

Opportunities in support of JCSDA may also be found at http://www.jcsda.noaa.gov/careers.php as they become available.

NOTE FROM THE DIRECTOR

The JCSDA is constantly looking for ways to collaborate better and operate more efficiently. In keeping with this philosophy, the Management Oversight Board (MOB) has recently approved a white paper describing a new concept of operations with improved management procedures. A key component is the Annual Operating Plan (AOP), which formalizes core funding and in-kind contributions from each partner and integrates them into a project-based structure with clear deliverables. The AOP will clarify the perimeter of JCSDA resources and activities, and it will increase accountability to the funding agencies. The current cross-agency elaboration of the AOP shows the value of coordinated planning in identifying overlaps, gaps, and issues.

Projects are designed to be flexible and adapted to the partners' needs. In this context, we are happy to bring onboard Guillaume Vernieres as project lead for the new project on Sea-ice, Ocean, Coupled Analysis (SOCA). Guillaume brings extensive expertise from his previous job at the NASA Global Modeling and Assimilation Office (GMAO). His mandate will involve integrating work across federal agencies to ensure maximum progress on ocean and sea-ice data assimilation. Welcome Guillaume!

As usual, the JCSDA is busy organizing events to accelerate the progress on satellite DA. The Unified DA Planning Meeting (April 4-5 in College Park, MD) will be an opportunity to collect requirements from the community regarding the next-generation DA and to draft a collaborative roadmap, which will support the needs of NOAA's Next-Generation Global Prediction System (NGGPS). The 15th JCSDA Technical Review Meeting and Science Workshop on Satellite DA (May 17-19 in College Park, MD) will bring together scientists from partner agencies and external research to review progress made in the past year. For the first time, it will be accompanied by the Community Radiative Transfer Model (CRTM) Users and Developers Workshop (May 16), highlighting the "Community" in the CRTM. We are also working with NOAA/NCEP/EMC and the Development Testbed Center (DTC) to jointly organize the next GSI/EnKF DA Tutorial in College Park this summer. Finally, as a member of the WMO Working Group on Data Assimilation and Observing Systems (DAOS), I would like to draw your attention to the 7th International WMO Symposium on Data Assimilation (September 11-15 in Florianopolis, Brazil) and its capacity to foster international collaborations aimed at advancing DA science.

Thomas Auligné
Director, JCSDA

SCIENCE CALENDAR

UPCOMING EVENTS

MEETINGS AND EVENTS SPONSORED BY JCSDA

DATE	LOCATION	TITLE
16 May, 2017	NOAA NCWCP, College Park, MD.	CRTM Users/Developers Workshop
17–19 May, 2017	NOAA NCWCP, College Park, MD.	JCSDA 15th Technical Review Meeting & Science Workshop on Satellite Data Assimilation
11–14 July, 2017	NOAA NCWCP, College Park, MD.	GSI/EnKF Community Tutorial*
TBD 2018	TBD	JCSDA Summer Colloquium on Satellite Data Assimilation

* Note from the GSI/EnKF Tutorial Organizing Committee: This tutorial will be a three and a half-day event. Lectures and hands-on sessions will be provided by invited speakers from major GSI and EnKF development teams on July 11-13 (Monday-Thursday), followed by an optional practical session on Friday morning (July 14).

All are invited to the GSI Workshop and the GSI Tutorial lecture portion. However, due to the constraints of physical space and staffing, we can only accommodate a maximum of 40 participants for the tutorial hands-on portion.

Registration will open by early April. Further details and information will be provided through the DTC website (http://www.dtcenter.org/) and the community GSI website (http://www.dtcenter.org/com-GSI/users/).

JCSDA seminars are generally held on the third Wednesday of each month at the NOAA Center for Weather and Climate Prediction, 5830 University Research Court, College Park, MD. Presentations are posted at http://www.jcsda.noaa.gov/JCSDASeminars.php prior to each seminar. Off-site personnel may view and listen to the seminars via webcast and conference call. Audio recordings of the seminars are posted at the website the day after the seminar. If you would like to present a seminar, contact Ling Liu, ling.liu@noaa.gov, or Biljana Orescanin, biljana.orescanin@noaa.gov.

MEETINGS OF INTEREST

DATE	LOCATION	WEBSITE	TITLE
23–28 April, 2017	Vienna, Austria	http://www.egu2017.eu	European Geosciences Union (EGU) meeting
25-26 April, 2017	Kansas City, MO.	http://www.testbeds.noaa.gov/events/2017/workshop/	8th NOAA Testbeds & Proving Grounds Workshop
27 April, 2017	Kansas City, MO.	http://www.goes-r.gov/users/2017GOES16FirstResultsWorkshop.html	GOES-16 The First Results Workshop
12–14 June 2017	Oslo, Norway	http://www.iris.no/enkf/enkf-homepage	12th EnKF workshop
31 July–2 August 2017	Vancouver, Canada	http://www.cs.ubc.ca/~greif/precon17/registration.html	Preconditioning 2017: International conference on preconditioning techniques for scientific and industrial applications
11–15 September 2017	Florianopolis, Brazil	http://www.cptec.inpe.br/das2017/	Seventh International WMO Symposium on Data Assimilation
29 November–5 December, 2017	Darmstadt, Germany	https://cimss.ssec.wisc.edu/itwg/itsc/itsc21/index.html	21st International TOVS Study Conference
11–15 December 2017	New Orleans, USA	http://fallmeeting.agu.org/2016/future-meetings/	American Geophysical Union Fall Meeting